



UNIVERSITY OF LEEDS

This is a repository copy of *A novel multiplex absorption spectrometer for time-resolved studies*.

White Rose Research Online URL for this paper:
<http://eprints.whiterose.ac.uk/126766/>

Version: Accepted Version

Article:

Lewis, T, Heard, DE orcid.org/0000-0002-0357-6238 and Blitz, MA
orcid.org/0000-0001-6710-4021 (2018) A novel multiplex absorption spectrometer for time-resolved studies. *Review of Scientific Instruments*, 89 (2). 024101. ISSN 0034-6748

<https://doi.org/10.1063/1.5006539>

(c) 2018, Author(s). This is an author produced version of a paper published in *Review of Scientific Instruments*. Uploaded in accordance with the publisher's self-archiving policy.

Reuse

Unless indicated otherwise, fulltext items are protected by copyright with all rights reserved. The copyright exception in section 29 of the Copyright, Designs and Patents Act 1988 allows the making of a single copy solely for the purpose of non-commercial research or private study within the limits of fair dealing. The publisher or other rights-holder may allow further reproduction and re-use of this version - refer to the White Rose Research Online record for this item. Where records identify the publisher as the copyright holder, users can verify any specific terms of use on the publisher's website.

Takedown

If you consider content in White Rose Research Online to be in breach of UK law, please notify us by emailing eprints@whiterose.ac.uk including the URL of the record and the reason for the withdrawal request.



eprints@whiterose.ac.uk
<https://eprints.whiterose.ac.uk/>

A novel multiplex absorption spectrometer for time-resolved studies.

Thomas Lewis¹, Dwayne E. Heard^{1,2}, Mark A. Blitz^{1,2,*}

School of Chemistry, University of Leeds, Leeds, LS2 9JT, UK

National Centre for Atmospheric Science, University of Leeds, Leeds, LS2 9JT, UK

* Corresponding author: m.blitz@leeds.ac.uk

ACCEPTED MANUSCRIPT

Abstract

A Time-Resolved Ultraviolet / Visible (UV/Vis) Absorption Spectrometer (TRUVAS) has been developed that can simultaneously monitor absorption at all wavelengths between 200 – 800 nm with millisecond time resolution. A pulsed photolysis laser (KrF 248nm) is used to initiate chemical reactions that create the target species. The absorption signals from these species evolve as the composition of the gas in the photolysis region changes over time. The instrument can operate at pressures over the range ~10 - 800 Torr and can measure time-resolved absorbances $<10^{-4}$ in the UV (300 nm) and even lower in the visible (580 nm) 2.3×10^{-5} , with the peak of sensitivity at ~500 nm. The novelty of this setup lies in the arrangement of the multipass optics. Although appearing similar to other multipass optical systems (in particular the Herriott cell) there are fundamental differences, most notably the ability to adjust each mirror to maximise the overlap between the probe beam and the photolysis laser. Another feature which aids the sensitivity and versatility of the system is the use of 2 high-throughput spectrographs coupled with sensitive line-array CCDs, which can measure absorbance from ~200-800 nm simultaneously. The capability of the instrument is demonstrated via measurements of the absorption spectrum of the peroxy radical, HOCH₂CH₂O₂ and its self-reaction kinetics.

I. INTRODUCTION

Absorption spectroscopy is widely used as a method of detecting molecules in gas, liquid and solid phase media. A common application of absorption spectroscopy is for gas-phase kinetic and spectroscopic measurements, since the technique allow time-resolved concentrations of species to be followed, particularly in the UV/Visible(Vis) region. The simplest UV-Vis absorption systems uses a single-pass, where the probe light travels directly from the source through a short length (typically <1 m) reaction cell containing the reaction mixture before reaching the detector.¹⁻⁴ The advantage of a single pass absorption system is that the intensity of the light that reaches the detector is normally high enough to access the full dynamic range of the detector. The probe light is typically from a lamp, which normally has some output in the UV, where most but not all species absorb. However, a lamp is inherently a divergent light source and is therefore difficult to deliver over a long distance, or in a multipass arrangement.

Traditionally, absorption systems of this type utilised a monochromator to select a narrow wavelength range (≤ 1 nm) from the lamp in order to follow changes in absorption over time that could be assigned to a specific species of the reacting system.^{4, 5} However, to fully characterise a system the experiment needs to be repeated for several wavelengths in order to assign the kinetics to a single, identified species. More recent advances have led to multiplexing absorption systems, where many wavelengths of light are recorded simultaneously by dispersing the light with a spectrograph onto a CCD camera as a function of time.⁶ How many wavelengths that are simultaneously recorded depend on the spectrograph, and is normally a trade-off between the wavelength range and resolution: in order to observe over hundreds of nanometers means that the resolution is ~ 1 nm.⁷⁻⁹

In general, the absorption of a molecule conforms to the Beer-Lambert law:

$$A = -\ln \frac{I}{I_0} = \sigma_{\lambda} \cdot c \cdot l \quad \text{E1}$$

where I and I_0 are the intensity of the light before and after absorption cell, respectively, and A is the absorbance, which linearly depends on σ_{λ} , c and l , the absorption cross-section at wavelength λ , concentration and pathlength, respectively. Since cross-sections are fixed and inherent to a given molecule, and concentration is determined by experimental factors (photolysis laser energy, precursor concentration etc.), then for sensitive detection it is desirable to extend the pathlength when probing via absorption, as the absorbance scales

linearly with l . Multipassing the probe light through the sample is a commonly employed technique to increase the absorbance measured in absorption experiments.

The White¹⁰⁻¹⁴ and Herriott^{10, 15-19} designs represent the two most often used optical arrangements utilised for the multipassing of probe light, where typically 8 to 100 passes are achieved. The White optical arrangement uses 3, focusing, independently adjustable mirrors, positioned such that incident probe light at one end closely passes by the single mirror to the two adjacent mirrors at the other end. This arrangement of mirrors multipasses the light, before finally exiting the single mirror. Herriott cells work in a similar manner, however with an optical arrangement containing only 2 mirrors, and the probe light is introduced through a hole in one of the mirrors, reflected through the sample between the 2 mirrors in a circular pattern, until the incident probe beam exits through a hole in the other mirror. The Herriot design requires a collimated light source, generally limiting its use for single-wavelength laser absorption spectroscopy. The White design is not as demanding but in general the size of the mirrors, and hence reaction cell, needs to be increased when multipassing incoherent lamp light. Another consideration is mounting the multipass optics inside or outside the reaction cell. The optimum number of passes is significantly higher when the multipass optics are inside the reaction cell as the losses per pass are limited by the reflectivity of the optics, which is typically ≥ 0.95 . Externally mounted multipass optics have additional losses because of passing the light through the reaction cell windows, which will typically reduce the effective reflectivity by an additional 0.10, i.e. overall reflectivity equal to 0.85 per pass. However, externally mounted optics will not be degraded by chemicals in the reaction cell and alignment will not change with pressure, which is often the case for internal optics. These considerations can outweigh the increased absorbance signal of internally mounted multipass optics.

The ultimate increase in pathlength is obtained when highly reflective mirrors ($R > 0.999$) are mounted inside the reaction cell and aligned to form a cavity, where the pathlength can be thousands of meters. Cavity ring-down spectroscopy (CRDS) is the most familiar cavity technique and has shown great success in measuring absorption for a variety of species at low concentration.²⁰⁻²³ It operates by introducing light into the optical cavity through the rear of one of a pair of highly reflective mirrors and measures the intensity of the light that exits the other mirror, where the change in light intensity is the “ring down time”. In general, CRDS optics are highly reflecting but operate over a narrow range of wavelengths (~ 50 nm).

First developed by Fiedler *et al.* in 2003²⁴, Incoherent Broad-Band Cavity-Enhanced Absorption Spectroscopy (IBB-CEAS) is a cavity technique that uses broad-band highly reflective mirrors to trap and multipass the probe radiation through the sample to enhance the effective path length of the absorption. The main difference with this technique is that the light source is from a lamp so that many wavelengths are multipassed by the cavity and are detected simultaneously on a CCD. This allows the full spectrum of a species to be recorded simultaneously, especially useful if the spectrum of the target has characteristic features that extends many nm. In general, IBB-CEAS mirrors are not as reflective as CRDS mirrors.

While cavities can increase the detection pathlength to > 1000 m, the increased detection sensitivity normally scales less than linearly with pathlength. In the case of IBB-CEAS the number of photons reaching the detector is normally much smaller than the dynamic range of the detector, and hence limits the minimum absorbance that can be measured. In the case of CRDS, the change in the “ring down time” is normally determined to no better than 1 part in 1000. In addition, cavity mirrors do not extend below 300 nm, and hence limits the wavelength range cavity techniques can be used. Another consideration when doing kinetics experiments is that the laser photolysis axis is normally not along the cavity-axis and it usually crosses the cavity axis at as small acute angle as possible in order to maximize the reaction zone sampled by the cavity; it usually only a few percent of the cavity length.²⁵

In this paper we describe a Time-Resolved Ultraviolet / Visible (UV/Vis) Absorption Spectrometer (TRUVAS) which uses an original multipass configuration that can access the dynamic range of a CCD detector on a millisecond timescale and overall enables a sensitive probe of time-resolved absorption over a wide wavelength range, 200 - 800 nm.

II. INSTRUMENTAL

A schematic of the instrumental setup is shown in Figure 1. There are 14 individually translatable mirrors, adjusted to direct the probe beam in such a way that overlap with the excimer beam, which is directed coaxial to the centre of the cell, is maximised. The reaction cell is a 1.5 m long glass tube, 54 mm OD, with 12 mm OD inlet and outlet ports, sealed with 3 mm thick fused silica windows at both ends. Additional to the multipass optical arrangement is a single-pass optical arrangement, which intersects the reaction volume only once. The probe light in this setup is produced by a Laser Driven Light Source (LDLS – Energetiq EQ-99X).

The LDLS is more suitable for this application than a standard Xe short arc lamp because the temperature of the spectral output is much higher (~ 11000 K vs 3000 K), producing near constant radiance from the NIR to the UV, < 200 nm. The output from the LDLS is extracted with an off-axis parabolic mirror that typically directs ~ 10 mW/cm² of light onto the first multipass mirror. The improved performance of the LDLS is partially due to its output variability being random, which is not always the case from a Xe arc lamp. The source is from a much smaller point (100 - 200 μm vs ~ 2 - 3 mm long), making the beam much easier to achieve collimation, via an off-axis parabolic mirror, over the long distances (up to ~ 20 m) required for this application.

Gases are flowed into a mixing manifold via 5 separate mass flow controllers (MFCs), the largest, Tylan (FC260-SA 10 slm) delivers the buffer gas N₂ (BOC, OFN), and a range of MKS flow controllers (Type 1179A, 3.5 SLM, 500 SCCM, 50 SCCM and 20 SCMM) for the O₂ (BOC, 99.5%) and other reagents (H₂O₂, 50 wt % in H₂O, Sigma / C₂H₄ technical grade, Air Products). Gas is evacuated from the cell by a 2-stage rotary pump (Edwards EM2), holding the cell at a typical pressure of ~ 50 - 100 Torr (cell pressure can be readily altered in the range 10 - 760 Torr).

The intensity of the probe radiation is recorded between 250 and 800 nm for the multipass arrangement and 200 to 600 nm for the single pass arrangement using a high throughput spectrograph (CP140-103, $f/2$) and a fast-read (1 kHz) line-array CCD (Hamamatsu S7031), which is significantly populated (10 - 100% of 65535 counts, depending on wavelength) for each millisecond time point to produce a 2D, time resolved absorption spectra. 248 nm radiation from a KrF excimer laser (Lambda-Physik CompEx 210) is directed along the cell using a dichroic turning mirror to initiate chemistry via the photolytic production of a radical from a suitable precursor. A TTL pulse from a delay generator (SRS DG535) first fires the camera, then the excimer laser after a delay of 1000 millisecond. The pulse repetition frequency of the excimer laser is selected to allow sufficient time for the illuminated reaction mixture to be pumped out of the cell, to be replaced by unprocessed reagents avoiding secondary photolysis of reaction products (repetition rate typically 0.2 Hz).

IIa. Optical Arrangement

The multipass optical arrangement used here is unreported in the literature, controlled by up to 14 mirrors (Knight Optical, UK) each of 12 mm diameter. The number of mirrors can be altered

for different applications and desired path lengths – typically 7 (pathlength = 443 cm) passes is optimal for measuring cross sections in the UV (250-400 nm), however up to 13 passes (pathlength = 700 cm) can be used if small cross sections in the visible region are to be measured. Each of the mirrors is adjustable, as shown in Figure 2, allowing for translation in the x and y axes (vertical and lateral), so that the overlap between the probe beam and the excimer beam can be maximised. The 12 mm diameter mirrors are spherically curved with a 2.4 m radius of curvature and are UV enhanced such that their reflectivity is $> 85\%$ in the UV (custom made by Knight Optical). The mounts were designed in SolidWorks® 2013 and consist of 2 aluminium back plates and 8 individual threaded mounting disks, onto which the mirrors are mounted. M3 screws hold the disks in place and silicone O-rings separate the threaded disks and mounting plate, which allows the angle of each mirror to be adjusted so that the probe beam can be arranged in the configuration outlined in Figure 1, which maximises overlap with the excimer beam along the axis of the cell. The final design of the mirror mount assembly, uses small O-rings to give the < 1 mm precise adjustment required, as shown in Figure 2.

The mounting plates and threaded disks were milled from aluminium by the School of Chemistry mechanical workshops and the optical mounts are fixed in place with custom made L-shaped brackets, which are slotted to allow vertical and horizontal translation of the mount assembly. To remove as much scattered excimer light as possible, whilst retaining probe intensity at short wavelengths (250-290 nm), a sharp cut-on filter (248 nm RazorEdge® ultrasteep long-pass edge filter – Semrock) is placed in the path of the beam, before the fibre-launcher (Elliot Scientific) for the multi-pass arrangement. For the single pass arrangement, light is directed through the hole in the top left corner of the mounting plate shown in Figure 2 and enters the spectrograph directly for optimum throughput of UV light (down to ~ 180 nm) with minimal pickup of excimer laser scattered light. In this mirror arrangement there are many multipass configurations that can be chosen, where maximum overlap with the excimer photolysis laser is the goal. The configuration chosen tried to have as many passes that cut diagonally through the volume illuminated in the reaction cell by the photolysis laser, see rectangular hole in Figure 2, right. It is not possible for all passes to cross diagonally, so each pass has a different pathlength associated with it.

Ib. The camera/spectrograph

The spectrographs (Horiba CP140-103, Imaging Spectrograph) used in this experimental setup have a wavelength range of ~ 600 nm. The camera collects the multipassed light over the wavelength range 250-850 nm, and the single pass camera ~ 185 -600 nm (the wavelength range is dictated by the mounting position of the camera on the exit of the spectrograph). This f/2 spectrograph yields high total light throughput with a wavelength resolution ~ 1.5 nm FWHM. High light throughput is desirable as exposures are typically less than or equal to 1 millisecond. With such short exposure times, more light is required to accumulate sufficient charge on the CCD pixels to see adequate signal for measuring absorption. The cameras used here are 16 bit line CCD detectors (Hamamatsu S7030-1006 FFT) which comprise an array of 1030 by 64 pixels. Charge which accumulates on pixels is binned and summed by the 64 vertical clocks (FFT – Full Frame Transfer) into the horizontal sum register. An important feature of this CCD chip is that the horizontal sum data are read off via the PCI interface board onto the computer at > 1000 Hz (780 μ s minimum read time). This means that the data is accumulated in real-time and there is no accumulation of “dark noise”, charge accumulation due to processes within the CCD itself. This means that expensive cooling of the camera is not necessary. Early versions of this type of experiment used 2D CCD array cameras that could not transfer the data in real-time, and therefore needed to be cooled as the data of the experiment accumulated on the CCD for many seconds before reading the 2D array at the end of the experiment.^{26,27} Faster 1D CCDs do exist, however they tend to be less efficient at collecting light per unit of time and therefore would result in an instrument with less sensitivity.²⁸ In all the work presented in this paper the exposure (sample) time of each pixel was set to 1 millisecond.

The CCD of the second camera used in this experiment is positioned on the spectrograph so that it can measure light 190 – 600 nm. When broadband light is passed through the fused silica windows of the reaction cell and reflected off the aluminium mirrors, $\sim 15\%$ of the light is lost. However, this loss is higher in the UV and increases the shorter the wavelength ($\sim 25\%$ loss at 260 nm), meaning the UV light which reaches the detector in the multipass system is much less intense than in the broadband light emitted from the LDLS light source. For this reason the single pass absorption arrangement is useful for retaining high intensity UV light for probing absorption at wavelengths shorter than 250 nm, simultaneously to the multipass absorption system. The cross-section of the collimated light from the LDLS is sufficiently large to provide both the multi and single pass light, which enters and exits the mirror mount plate via the large circular aperture, see Figure 2.

The absorption setup also has a non-time resolved mode whereby the absorption of stable molecules can be determined in the absence of the excimer laser radiation. This is achieved by measuring light intensity in the presence and absence of the analyte present, using the same camera for both I and I_0 . The primary application of the stable molecule mode is to quantify the concentration of the photolysis precursor, using equation E1, in the absence of the laser, which is in turn used to quantify the concentration of the radicals being probed where the probe pathlength is the cell length (150 cm) multiplied by the number of passes.

The cameras, spectrographs, fibre optics and data transfer PCI interface board were supplied by Entwicklungsbüro Stresing.²⁸

IIIc. Data processing

Data are transferred from the camera to the computer via the dedicated PCI interface board supplied with the camera. The transfer rate of the PCI board is sufficiently fast to read the data in real time, and the data are fed into a LabVIEW® program coded here at the University of Leeds, which converts the raw 2D array, which is in the form of Pixel number vs. time, into wavelength vs. time, where for any given pixel there is the number associated with it equal to the intensity of light it has accumulated and is the third-axis, see Figure 5. The intensity of the light prior to t_0 (excimer laser firing) is averaged and represents I_0 , and the intensity of the light subsequent to t_0 represents I . A cut through the 2D array can be taken through the wavelength axis to view the spectrum at a given time delay, which have x and y assignments of wavelength and absorbance respectively. Alternatively, for kinetic applications, cuts through the time axis gives the time evolution of the total absorbance change for any given wavelength, see Figure 5.

To account for fluctuations in lamp intensity, the variation in absorbance for a wavelength region where no absorption occurs (typically 500-600 nm and is referred to as the “pinning region”) is assumed to be purely due to lamp fluctuations (see black trace in Figure 3). This fluctuation can be used to normalise the data over all wavelength and in the pinning region forces A to be equal to 0. Fixing A to 0 to a wavelength region where it is reasonable to assume no absorption is a simple way to reduce the noise due to lamp fluctuations, as demonstrated in Figure 3, which in turn reduces the number of excimer shots required to obtain a satisfactory signal.

IV. PERFORMANCE OF THE SYSTEM

IVa. Effective path length

Whilst the mirror multipass configuration is set up to optimise the overlap between the lamp probe beam and the excimer laser beam, Figure 1 shows that complete overlap inside the cell is not possible, and hence the path length for photolytic experiments is not equal to the length of the cell multiplied by the number of passes. For this reason, it is necessary to measure the extent of the overlap between the excimer and the probe beams, which is achieved by photolysing isopropyl nitrate ($i\text{PrNO}_3 = (\text{CH}_3)_2\text{CHONO}_2$) to yield NO_2 with a known quantum yield of near unity (R1).^{8, 29, 30}



The magnitude of the NO_2 absorbance is measured using the multipass arrangement, and simultaneously in a single pass coaxially along the excimer beam, as illustrated in Figure 4.

The measurement of the absorbance coaxial to the excimer laser beam, A_{coaxial} , has a well constrained path length equal to the length of the cell (150 cm), making it possible to then calculate the effective path length, $l_{\text{multipass}}$ using equations E2 and E3:

$$\frac{A_{\text{coaxial}}}{l_{\text{coaxial}}} = \frac{A_{\text{Multipass}}}{l_{\text{multipass}}} \quad \text{E2}$$

$$l_{\text{multipass}} = l_{\text{coaxial}} \cdot \frac{A_{\text{Multipass}}}{A_{\text{coaxial}}} \quad \text{E3}$$

This single pass along the reaction cell, l_{coaxial} , to calibrate the pathlength works well for NO_2 as its spectrum is very broad and centred about 400 nm and that the NO_2 probing light is transmitted through the dichroic 248 nm excimer mirror. This transmitted probe light is shaped so that it was always inside the volume mapped out by the photolysis light. This calibration is independent of the NO_2 quantum yield of reaction R1, subsequent NO_2 kinetics and $[i\text{PrNO}_3]$, even though it was determined before each photolysis experiment using the stable molecule part of the data collection program. The multipass path length was determined to be 443 ± 21 cm for 7 passes and 700 ± 100 cm for the 13 pass configuration, using this method. The errors were determined by repeating this calibration experiment several times. NO_2 is a suitable molecule for this application due to its strong, structured absorption in the visible region. In

these experiment the absorbance was determined using all the visible wavelengths. The short-wavelength single pass arrangement, see Figure 1, cuts across the reaction cell at a small angle and its pathlength was assigned by comparison to the multipass pathlength and is equal to 58 ± 6 .

IVb. RO₂ absorption spectra.

The new UV-VIS time resolved absorption spectrometer described here has been constructed to initially measure absorption cross sections of organic peroxy radicals. Peroxy radicals are measured in this system by photolysing an OH precursor (H₂O₂) at 248 nm (R2) in the presence of an alkene and molecular oxygen. The OH molecule adds to one side of the double bond (R3) followed by the addition of oxygen to the other side of the double bond (R4).

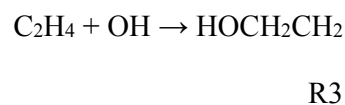


Figure 5 shows an example 2D time-resolved absorption spectrum of the ethylene hydroxyperoxy radical, HOCH₂CH₂O₂, and its subsequent kinetic behaviour.

The ability to measure absorption cross sections at wavelengths longer than 295 nm is important as it is only these wavelengths that reach the troposphere, and hence bring about photochemistry. Photolysis rates by sunlight of atmospheric radicals and molecules is the product of the cross-section (decreasing with wavelength, see Figure 5) and the photon flux (increasing with wavelength in the UV) summed over all wavelengths. In general, small cross sections ($<1 \times 10^{-19} \text{ cm}^2 \text{ molecule}^{-1}$) for peroxy radicals have not previously been determined due the lack of sensitivity of these absorption instruments. The present instrument has increased sensitivity because of the increased pathlength, stability of the probe light and the “pinning region”, where the wide wavelength range of the spectrograph means that there is almost always a region where there is no absorption. Figure 6 shows the absorption cross-sections for the ethylene hydroxyperoxy radical measured by the TRUVAS instrument, compared to the IUPAC recommendation by Lightfoot et al.³¹ Good agreement is observed at all wavelengths $\leq 290 \text{ nm}$. The cross-sections have been assigned by a simple, small extrapolation of the data in Figure 5 to time zero. The agreement provides validation of the accuracy of the cross section

measurements made by the TRUVAS instrument, and highlights the improved sensitivity and resultant smaller limit of detection compared to existing systems.³¹

IVc. Minimum Determination of the Absorption Cross-Section

Reactions 2, 3 and 4 in the presence of the excess C₂H₄ and O₂ lead to fast (sub-millisecond) and near complete conversion of OH to HOCH₂CH₂O₂ radicals. The longest wavelength where absorbance can be assigned to HOCH₂CH₂O₂ is a good measure of the sensitivity of the instrument, see Figure 6. However, the minimum cross section that can be measured should be calculable via the known amount of radicals that can be produced, see directly below, and the limit of detection, LOD, next section.

A is calculated via the Beer-Lambert law, Equation E1, and at low A (<0.05) for a given pathlength is proportional to cross-section multiplied by the concentration. Therefore to calculate the amount of OH generated from the 248 nm photolysis of H₂O₂, R2, requires $\sigma_{\text{H}_2\text{O}_2, 248 \text{ nm}}$ (known from the literature) and $[\text{H}_2\text{O}_2]$ (determined via the stable molecule program and is $\leq 10^{16}$ molecule cm⁻³). I/I_0 is typically 10^{-3} cm⁻¹, the fraction of photons absorbed per cm, and the energy of the excimer is typically ≤ 100 mJ / cm², which translates to $\leq 10^{17}$ photons/cm² per laser pulse. This means that the number of photons is insignificantly changed from the beginning to the end of the reaction cell. Therefore to a good approximation the OH concentration in these experiments is equal to:

$$[\text{OH}] = \sigma_{\text{H}_2\text{O}_2, 248 \text{ nm}} \times [\text{H}_2\text{O}_2] \times [h\nu]_{248\text{nm}} \times \Phi_{\text{OH}} \quad \text{E4}$$

where $[h\nu]_{248\text{nm}}$ is the excimer laser fluence and is determined via measuring the laser energy and Φ_{OH} is the OH quantum yield from R3, and is equal to 2 at 248 nm. The excimer energy is measured using a calibrated energy meter (Molelectron, JMAX 11). The sensor of the energy meter is 1 cm in diameter and this is smaller than that the excimer beam profile, rectangular and approximately 12 mm wide, and 30 mm high, which means that an accurate and reproducible energy can be determined.

The Limit of Detection (LOD) of the system is determined by the level of noise relative to the signal, the Signal to Noise Ratio (SNR). To see a signal-to-noise ratio of ≥ 1 the signal must be at least as big as the random noise experienced by the system, therefore the LOD is equal to the level of noise on the absorption signal. In the absence of any reagents or photolysis pulse,

I and I_0 are equivalent, and should produce absorbance values equal to 0. Deviation of the absorption away from 0 in this case is due exclusively to the noise experienced by the system. The standard deviation of (indicative of noise level) of the absorbance signal in the experiment at 580 and 300 nm was probed, and found to be 2.3×10^{-5} and 5.5×10^{-5} respectively after 2000 camera shots. Figure 7 shows how the standard deviation of the absorbance in the absence of an absorber decreases as a function of the number of camera samples of the probe light.

If the SNR is to be equal to 1, then the observed absorption (at 300 nm) must be greater than or equal to the noise:

$$\sigma_{min} \cdot c \cdot l \geq 5.5 \times 10^{-5} \quad \text{E5}$$

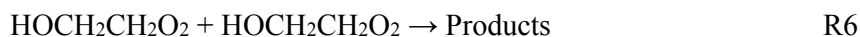
which implies the minimum cross section detectable at 300 nm by the system at a typical radical concentration of 5×10^{13} molecule cm^{-3} (radical concentrations generated in this experiment are in the range $3\text{-}9 \times 10^{13}$ molecule cm^{-3}) and a path length of 442 cm, is equal to:

$$\sigma_{min} \geq \frac{5.5 \times 10^{-5}}{c \cdot l} = \frac{5.5 \times 10^{-5}}{5 \times 10^{13} \times 442} = 2.4 \times 10^{-21} \text{ cm}^2 \text{ molecule}^{-1}$$

This value is significantly lower (\sim factor of 5) than given in Figure 6 but this is expected as the experiments in Figure 6 were a result of fewer samples, typically 200.

IVd. Kinetics

The highest time-resolution of the system is 780 μs /point. Therefore the system should be able to reliably determine kinetics $\leq 1/780 \times 10^{-6} = 1280 \text{ s}^{-1}$, i.e. the half-life of the molecule being monitored is greater than the time-resolution of the system. The loss kinetics in Figure 5 is mainly due to radical self-reaction:



Fitting the wavelengths of Figure 5 to self-reaction kinetics, R6, plus a first-order term to allow for diffusion of $\text{HOCH}_2\text{CH}_2\text{O}_2$ out of the photolysis volume, yielded $k_6 = 2.33 \pm 0.03 \times 10^{-12} \text{ cm}^3 \text{ molecule}^{-1} \text{ s}^{-1}$, which is in good agreement with the literature rate constant for R6 of $2.3 \times 10^{-12} \text{ cm}^3 \text{ molecule}^{-1} \text{ s}^{-1}$.³¹ The returned diffusion rate constant was $< 1 \text{ s}^{-1}$. However, it is noted that the returned value k_6 is perturbed if HO_2 is a significant reaction product and it reacts with $\text{HOCH}_2\text{CH}_2\text{O}_2$. In general, at pressures > 50 Torr diffusion is a few s^{-1} and needs to be accounted for in the data analysis. In Figure 3, the observed loss is slow and probably has a significant contribution from diffusion. Increasing the total pressure of the experiment is

straightforward and does not affect the quality of the data, but it is a simple way to minimize diffusion and hence better identify the chemical contribution to the kinetics. Also, as can be seen in Figure 5, the kinetics are occurring on the 10s of millisecond timescale for $k_6 = 2.33 \pm 0.03 \times 10^{12} \text{ cm}^3 \text{ molecule}^{-1} \text{ s}^{-1}$. Therefore, even if peroxy radical self-reaction were occurring at the collision frequency (corresponding to a rate coefficient of $\sim 10^{10} \text{ cm}^3 \text{ molecule}^{-1} \text{ s}^{-1}$) it would still not have a half-life approaching the highest time-resolution of the system. The peroxy radical concentration can also be reduced to increase the timescale of the kinetics.

The simplest Criegee intermediate, CH_2OO , has a strong, broad absorption spectrum centred $\sim 350 \text{ nm}$, which means it is convenient for detection. In the present experimental setup, $[\text{CH}_2\text{OO}] = 1 \times 10^{11} \text{ molecule cm}^{-3}$ yields an absorbance, A , equal to $\sim 10^{-3}$. So even though CH_2OO self-reaction is close to the gas-kinetic frequency:^{32, 33}



it can be conveniently detected with a lifetime ≥ 10 milliseconds. Therefore there is still a good dynamic range in order to carrying out bimolecular CH_2OO reaction kinetics. In fact, the first reaction this system studied was the reaction between CH_2OO and water vapour:



where the removal kinetics via R8 could be reliably measured up to $\sim 1500 \text{ s}^{-1}$.³⁴ The limit of the system to measure kinetics is reached for species that react with its precursor close to the gas-kinetic frequency, especially if the absorbing species have a small cross-section.

V. CONCLUSIONS

A novel TRUVAS instrument has been designed, which can measure absorption spectra between $\sim 200 - 800 \text{ nm}$ simultaneously, with a highest time resolution of $780 \mu\text{s}$. The pathlength of the instrument is increased by a novel multipass optical arrangement, which can give up to 13 passes, which yields a photolysis detection pathlength equal to 700 cm . The minimum absorbance that can be determined is equal to 2.3×10^{-5} (at 580nm), but is a factor of two worse in the UV, see Figure 7. The increased pathlength and reduced minimum A means that this TRUVAS instrument has at least a factor of 10 increased sensitivity for radical detection compared to previous time resolved UV-Vis absorption instruments, see Figure 6. Its sensitivity is comparable to a recent cavity instrument.²⁵ The broad range of wavelengths able

to be probed by this instrument is an important feature as it facilitates the simultaneous measurement of the whole UV/VIS spectrum of a single species and its kinetics, or kinetic measurement of multiple species, and the quality of the data is improved as there is almost always a region of no absorption so “pinning” can be applied. The TRUVAS experiment outlined here has already proven to be a powerful instrument for elucidating absorption cross sections of transient species, as well as kinetic parameters for important atmospheric reactions.^{34, 35}

ACKNOWLEDGEMENTS

This work was funded by a grant from the Natural Environment Research Council (grant NE/K005820/1) and the National Centre for Atmospheric Science.

ACCEPTED MANUSCRIPT

REFERENCES

- ¹ A. A. Jemi-Alade, P. D. Lightfoot and R. Lesclaux, *Chemical Physics Letters*, **179**, 119, (1991).
- ² R. A. Cox and R. G. Derwent, *Journal of Photochemistry*, **6**, 23, (1976).
- ³ M. E. Jenkin, T. P. Murrells, S. J. Shalliker and G. D. Hayman, *Journal of the Chemical Society, Faraday Transactions*, **89**, 433, (1993).
- ⁴ T. P. Murrells, M. E. Jenkin, S. J. Shalliker and G. D. Hayman, *Journal of the Chemical Society, Faraday Transactions*, **87**, 2351, (1991).
- ⁵ C. Yan, S. Kocевska and L. N. Krasnoperov, *Journal of Physical Chemistry A*, **120**, 6111, (2016).
- ⁶ D. M. Rowley, M. H. Harwood, R. A. Freshwater and R. L. Jones, *J. Phys. Chem.*, **100**, 3020, (1996).
- ⁷ D. Johnson, S. Raoult, R. Lesclaux and L. N. Krasnoperov, *Journal of Photochemistry and Photobiology A: Chemistry*, **176**, 98, (2005).
- ⁸ R. Talukdar, J. Burkholder, M. Gilles and J. Roberts, *Journal of the Chemical Society, Faraday Transactions*, **93**, 2797, (1997).
- ⁹ D. K. Papanastasiou, V. C. Papadimitriou, D. W. Fahey and J. B. Burkholder, *Journal of Physical Chemistry A*, **113**, 13711, (2009).
- ¹⁰ C. Robert, *Applied Optics*, **46**, 5408, (2007).
- ¹¹ J. U. White, *Journal of the Optical Society of America (1917-1983)*, **32**, 285, (1942).
- ¹² F. Wicktor, A. Donati, H. Herrmann and R. Zellner, *Physical Chemistry Chemical Physics*, **5**, 2562, (2003).
- ¹³ D. Tan, I. Faloon, J. B. Simpas, W. Brune, P. B. Shepson, T. L. Couch, A. L. Sumner, M. A. Carroll, T. Thornberry, E. Apel, D. Riemer and W. Stockwell, *Journal of Geophysical Research: Atmospheres*, **106**, 24407, (2001).
- ¹⁴ S. Himmelmann, J. Orphal, H. Bovensmann, A. Richter, A. Ladstätter-Weissenmayer and J. P. Burrows, *Chemical physics letters*, **251**, 330, (1996).
- ¹⁵ D. R. Herriott and H. J. Schulte, *Applied Optics*, **4**, 883, (1965).
- ¹⁶ J. Altmann, R. Baumgart and C. Weitkamp, *Applied Optics*, **20**, 995, (1981).
- ¹⁷ B. Wert, A. Fried, S. Rauenbuehler, J. Walega and B. Henry, *Journal of Geophysical Research: Atmospheres (1984–2012)*, **108**, (2003).
- ¹⁸ J. S. Pilgrim, R. T. Jennings and C. A. Taatjes, *Review of scientific instruments*, **68**, 1875, (1997).
- ¹⁹ J. B. McManus, M. S. Zahniser, D. D. Nelson, L. R. Williams and C. E. Kolb, *Spectrochimica Acta Part A: Molecular and Biomolecular Spectroscopy*, **58**, 2465, (2002).
- ²⁰ D. B. Atkinson, *Analyst*, **128**, 117, (2003).

- ²¹ D. B. Atkinson and J. L. Spillman, *Journal of Physical Chemistry A*, **106**, 8891, (2002).
- ²² M. B. Pushkarsky, S. J. Zalyubovsky and T. A. Miller, *Journal of Chemical Physics*, **112**, 10695, (2000).
- ²³ S. Wu, P. Dupre and T. A. Miller, *Physical Chemistry Chemical Physics*, **8**, 1682, (2006).
- ²⁴ S. E. Fiedler, A. Hese and A. A. Ruth, *Chemical Physics Letters*, **371**, 284, (2003).
- ²⁵ L. Sheps, *Journal of Physical Chemistry Letters*, **4**, 4201, (2013).
- ²⁶ J. C. Gómez Martín, P. Spietz, J. Orphal and J. P. Burrows, *Spectrochimica Acta Part A: Molecular and Biomolecular Spectroscopy*, **60**, 2673, (2004).
- ²⁷ W. J. Bloss, D. M. Rowley, R. A. Cox and R. L. Jones, *Physical Chemistry Chemical Physics*, **4**, 3639, (2002).
- ²⁸ G. Stresing, Entwicklungsburo Stresing, <http://www.stresing.de/>.
- ²⁹ K. C. Clemitshaw, J. Williams, O. V. Rattigan, D. E. Shallcross, K. S. Law and R. Anthony Cox, *Journal of Photochemistry and Photobiology A: Chemistry*, **102**, 117, (1997).
- ³⁰ L. Zhu and D. Kellis, *Chemical Physics Letters*, **278**, 41, (1997).
- ³¹ P. D. Lightfoot, R. A. Cox, J. N. Crowley, M. Destriau, G. D. Hayman, M. E. Jenkin, G. K. Moortgat and F. Zabel, *Atmospheric Environment. Part A. General Topics*, **26**, 1805, (1992).
- ³² Z. J. Buras, R. M. I. Elsamra and W. H. Green, *J. Phys. Chem. Lett.*, **5**, 2224, (2014).
- ³³ W. L. Ting, C. H. Chang, Y. F. Lee, H. Matsui, Y. P. Lee and J. J. M. Lin, *J. Chem. Phys.*, **141**, (2014).
- ³⁴ T. R. Lewis, M. A. Blitz, D. E. Heard and P. W. Seakins, *Physical Chemistry Chemical Physics*, **17**, 4859, (2015).
- ³⁵ R. F. Hansen, T. R. Lewis, L. Graham, L. K. Whalley, P. W. Seakins, D. E. Heard and M. A. Blitz, *Physical Chemistry Chemical Physics*, (2017).

FIGURE CAPTIONS

Figure 1: A schematic of the experimental setup. The Laser Driven Light Source (LDLS) is collimated by an off-axis parabolic (OAP) mirror. This light is split into the yellow beam for the multipass optical arrangement, and the red beam for the single pass optical arrangement. The single and multipass beams are subsequently detected by separate spectrograph/cameras before being passed to the computer via a fibre optic / PCI interface board. The excimer laser passes along the centre of the reaction cell containing the reagent gases and significantly crosses the probe beams.

Figure 2: A schematic of the mirror mount design. Left, the M3 screws are fed through the back plate, through the silicone O-rings, and screwed into the threaded mirror mounting plate. Middle is front view of an individual mirror mount. Right is the plate where seven mirrors are mounted, the orange represents the O-ring and shows the position of a mirror mount, the small holes are for the M3 screws, the large round hole is for the single pass and the rectangular hole is to allow the excimer laser to pass through it into the reaction cell. Mirrors are adhered to the mounting plate with Superglue.

Figure 3: An example of the effect of pinning on a time resolved absorption trace (1 ms time resolution, wavelength = 325 nm). The black trace is unpinned, raw data and the red trace is pinned using the 500 - 600 nm region, where the absorbing species (isoprene hydroxyperoxy radical) has a negligible absorption cross section, reducing the noise due to fluctuations in lamp intensity. The red trace displays significantly less random fluctuation in lamp intensity compared to the black trace, see text for further details. Conditions: $[\text{H}_2\text{O}_2] = 6.4 \times 10^{15} \text{ molecule cm}^{-3}$; $[\text{OH}] = 7.6 \times 10^{13} \text{ molecule cm}^{-3}$; total pressure = 82 Torr. [Isoprene] was $> 10 \times [\text{H}_2\text{O}_2]$ and the excimer energy was $52.3 \text{ mJ pulse}^{-1} \text{ cm}^{-2}$.

Figure 4: Multipass arrangement (top, black trace) and single pass coaxial arrangement along the excimer laser beam (bottom, red trace). Note, the coaxial beam overlaps with the excimer beam for the entirety of the length of the cell. OAP = off-axis parabolic mirror.

Figure 5: A 2-dimensional time and wavelength-resolved absorption spectrum (left) of the $\text{HOCH}_2\text{CH}_2\text{O}_2$ radical. Absorbance decay traces (top right) for the removal of the $\text{HOCH}_2\text{CH}_2\text{O}_2$ radical by self-reaction over a range of wavelengths, and absorbance as a function of wavelength at a range of time delays (bottom right). Conditions: $[\text{H}_2\text{O}_2] = 4.67 \times 10^{15} \text{ molecule cm}^{-3}$; $[\text{OH}] = 7.23 \times 10^{13} \text{ molecule cm}^{-3}$; total pressure = 239 Torr. $[\text{C}_2\text{H}_4]$ was $> 100 \times [\text{H}_2\text{O}_2]$ and the excimer energy was $68.2 \text{ mJ pulse}^{-1} \text{ cm}^{-2}$. Fits to the 260 – 300 nm data yielded $k_6 = 2.33 \pm 0.06 \times 10^{12} \text{ cm}^3 \text{ molecule}^{-1} \text{ s}^{-1}$, which is in good agreement with the literature.³¹

Figure 6: $\text{HOCH}_2\text{CH}_2\text{O}_2$ absorption cross sections. The solid blue line represents the cross sections from the fit to the single pass TRUVAS data. The multipass cross sections, red, and its error bars are assigned equal to the variability from repeated experiments. The crosses represent cross sections measured by Lightfoot *et al.*³¹ Currently the smallest measured cross sections in the literature are around $7.7 \times 10^{-19} \text{ cm}^2 \text{ molecule}^{-1}$ at 300 nm. The experimental data obtained using this instrument measure the $\text{HOCH}_2\text{CH}_2\text{O}_2$ cross section down to $\sim 2.2 \times 10^{-20}$ at $\sim 340 \text{ nm}$, which represents in excess of an order of magnitude greater sensitivity compared to previous measurements. This data were obtained from experiments where $[\text{H}_2\text{O}_2]$,

[OH] and total pressure (N_2) were varied over the ranges $3.7\text{--}9.7 \times 10^{13}$, $2.1\text{--}7.7 \times 10^{15}$ and $4.1\text{--}7.8 \times 10^{18}$ molecule cm^{-3} , respectively. $[C_2H_4]$ was $> 100 \times [H_2O_2]$ and the excimer energy was between $50\text{--}75$ $\text{mJ pulse}^{-1} \text{cm}^{-2}$.

Figure 7: The standard deviation of the absorption signal as a function of the number of camera samples at 300 nm (black) and 580 nm (red). The inset is a log-log plot that shows that the standard deviation has fallen to roughly 5.5×10^{-5} (300nm) and 2.2×10^{-5} (580 nm) after ~ 2000 1 millisecond samples. The camera triggered at a similar rate as the experiment, 0.2 Hz, with light after 13 passes of an empty reaction cell, where at 580 and 300 nm typically 50000 and 10000 photon counts were detected per sample, respectively.

ACCEPTED MANUSCRIPT

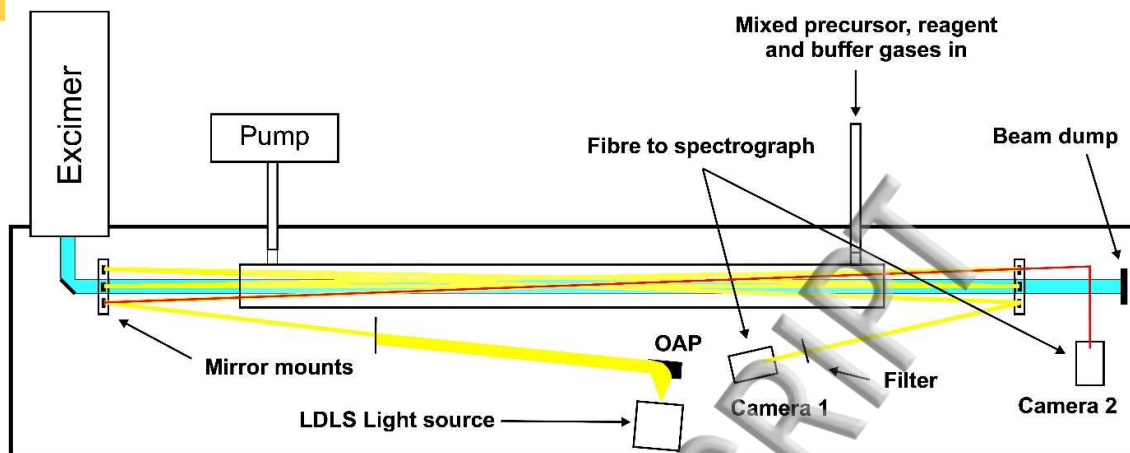


Figure 1

ACCEPTED MANUSCRIPT

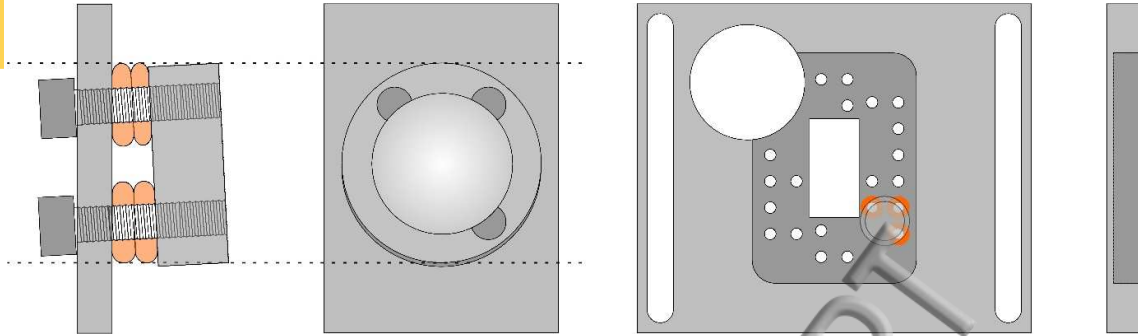


Figure 2

ACCEPTED MANUSCRIPT

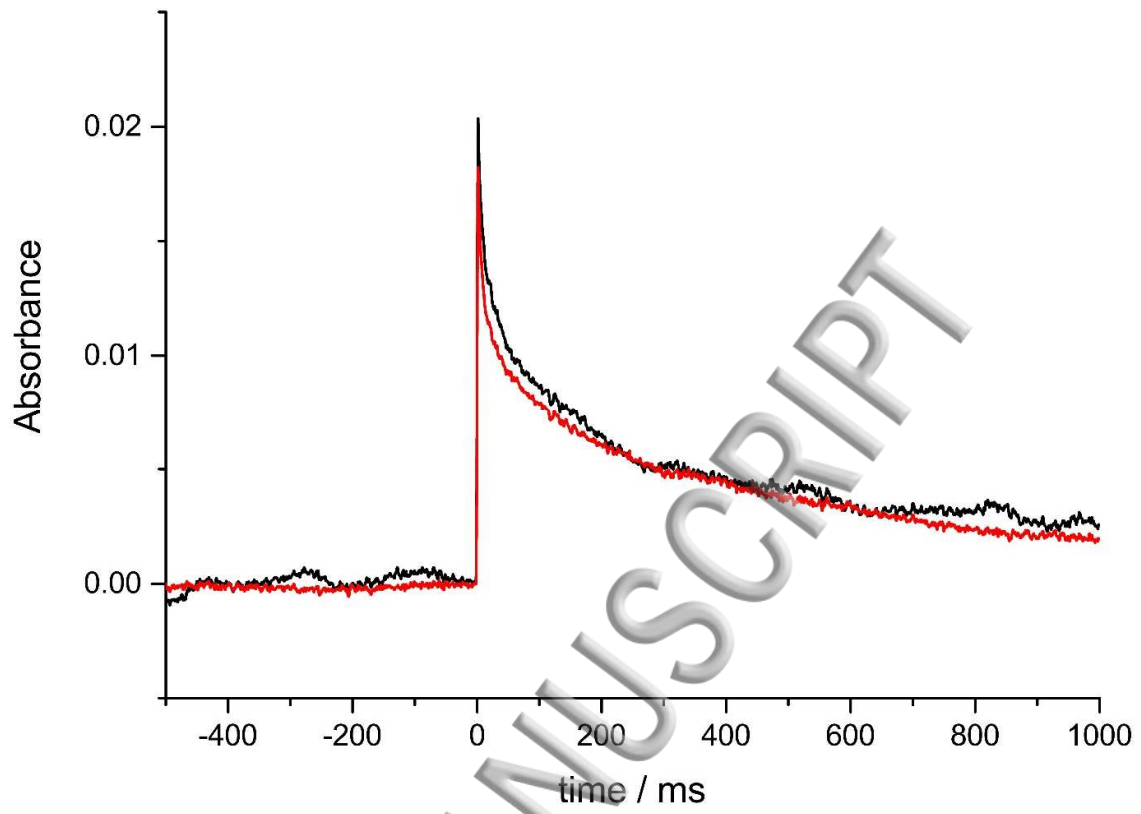


Figure 3.

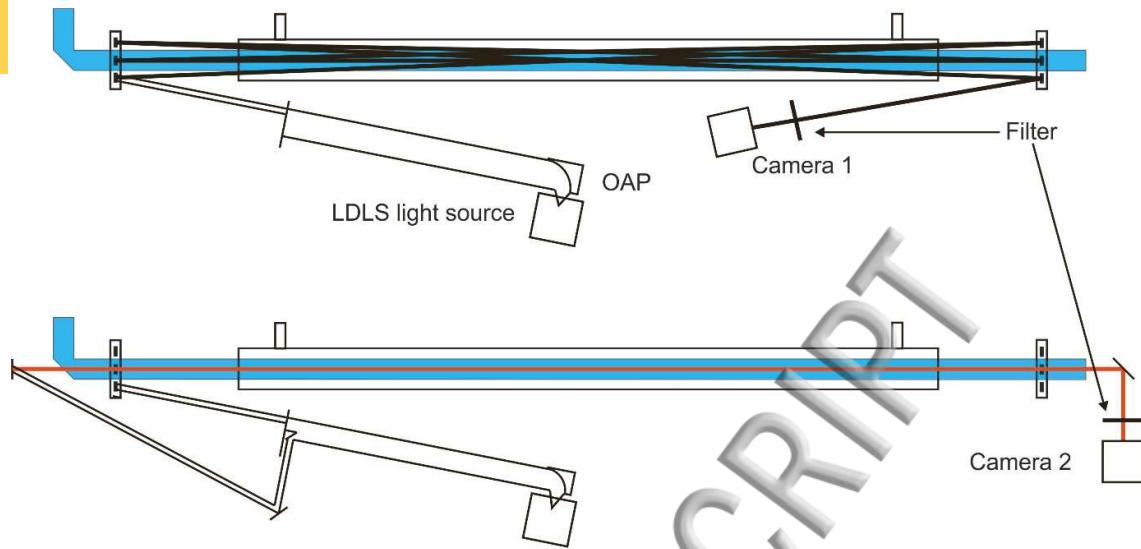


Figure 4.

ACCEPTED MANUSCRIPT

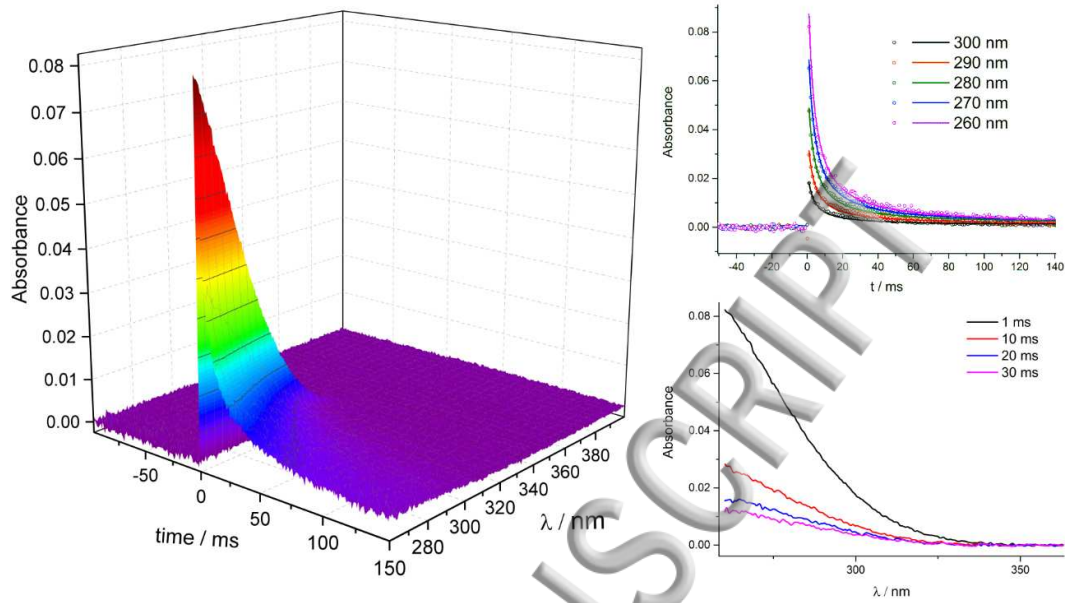


Figure 5.

ACCEPTED MANUSCRIPT

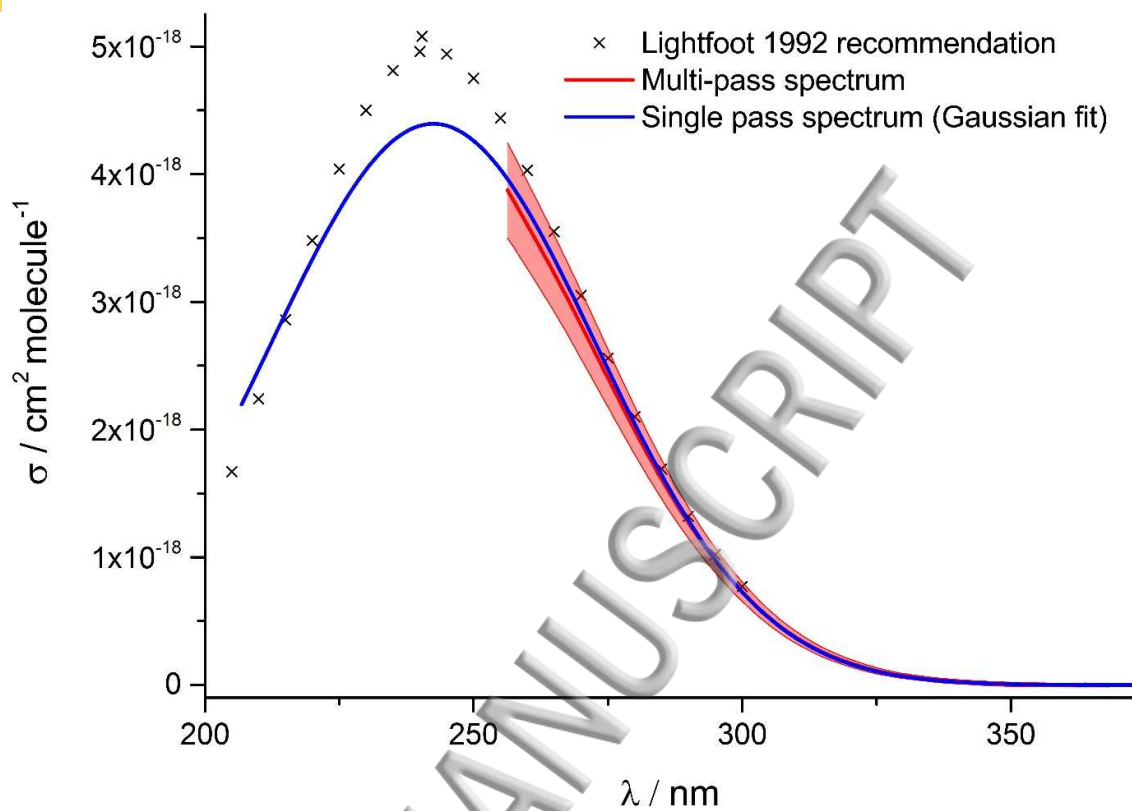


Figure 6.

ACCEPTED MANUSCRIPT

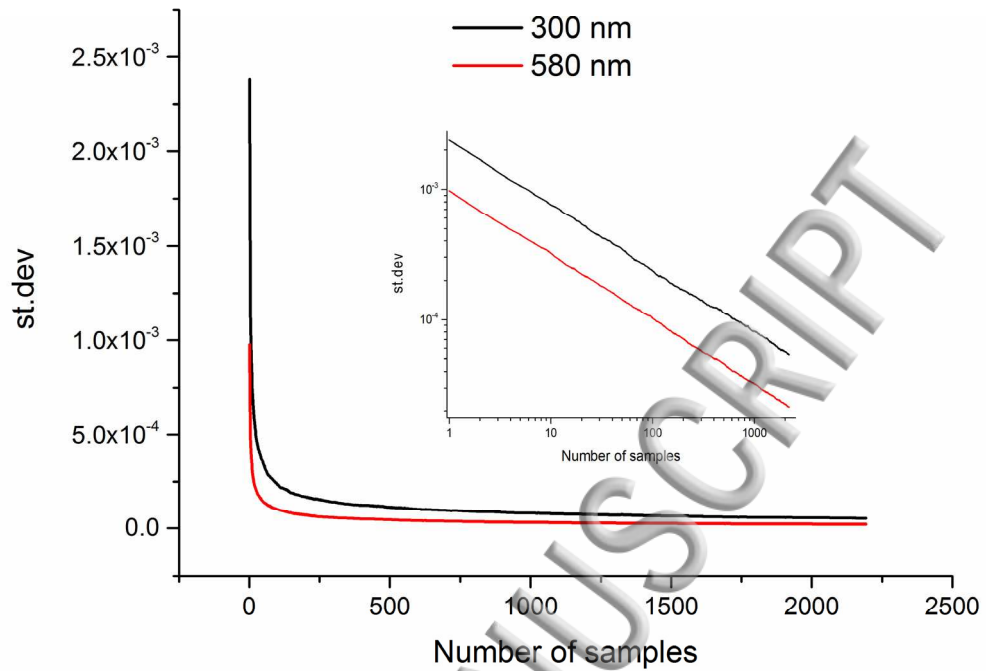
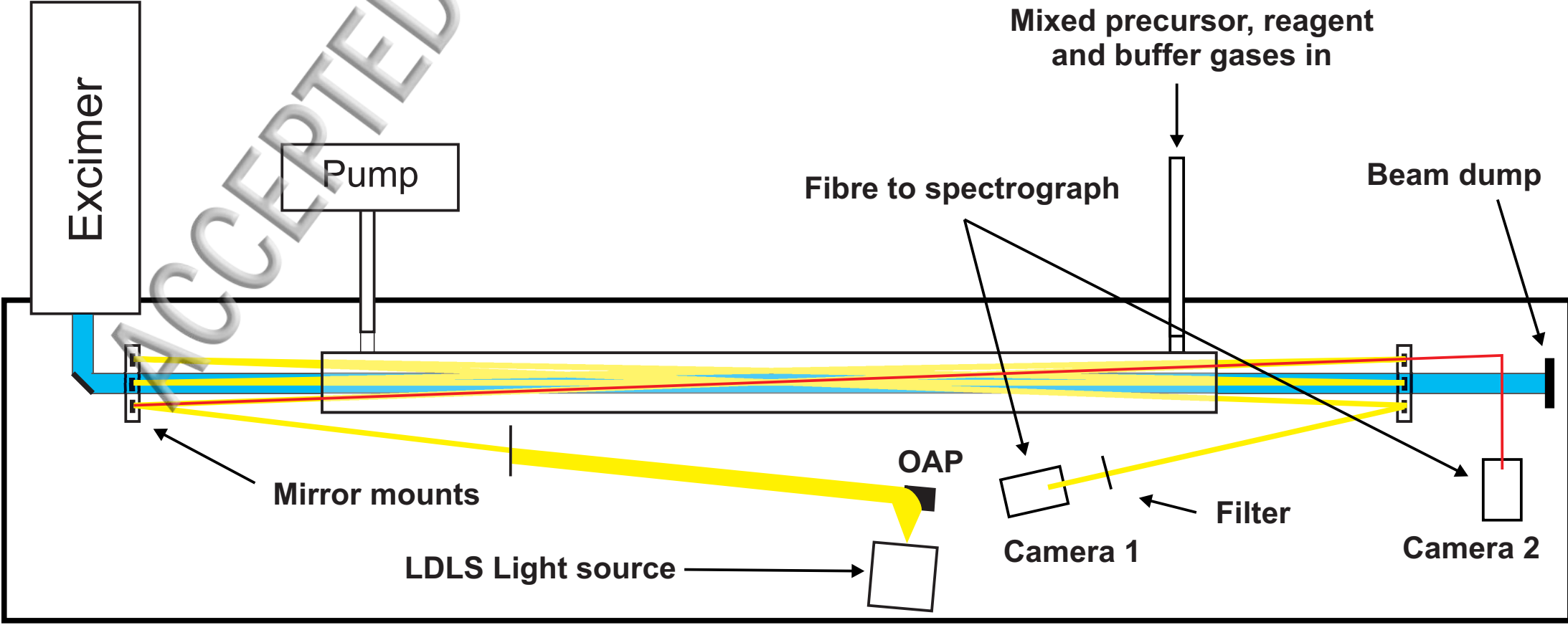
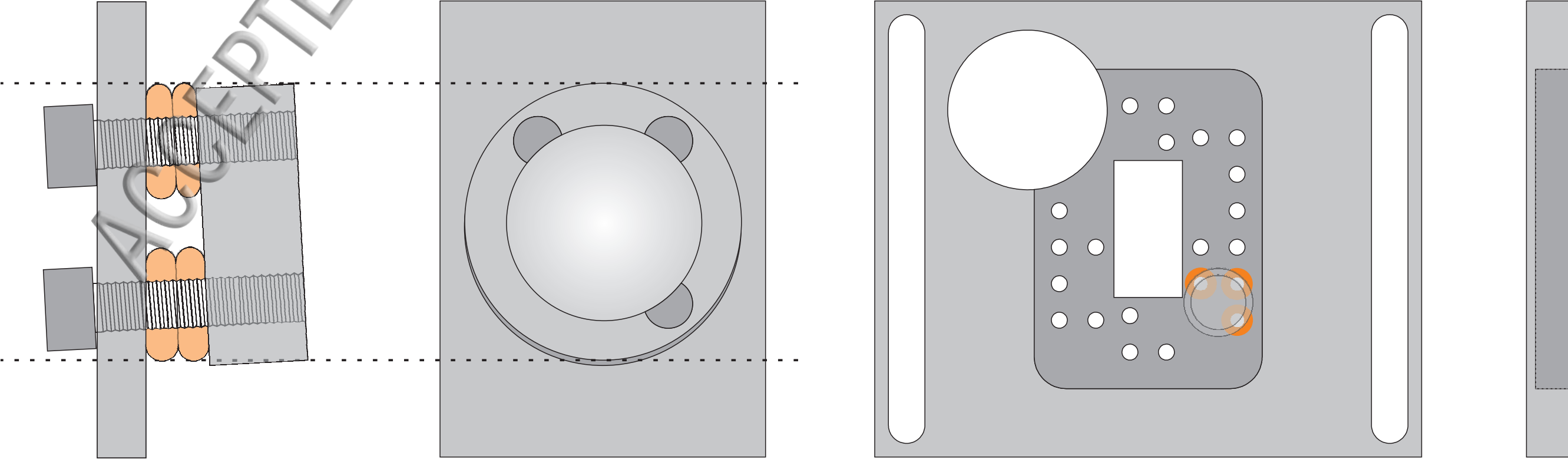


Figure 7.





Absorbance

0.02

0.01

0.00

-400

-200

0

200

400

600

800

1000

time / ms

